Supporting Information

Single-step conversion of ethanol to n-butene over $Ag\text{-}ZrO_2/SiO_2$ catalysts

Vanessa Lebarbier Dagle[a*], Austin D. Winkelman[a,b], Nicholas R. Jaegers[a,b], Johnny Saavedra-Lopez[a], Jianzhi Hu[a], Mark H. Engelhard[c], Susan E. Habas[d], Sneha A. Akhade[a,e], Libor Kovarik[a], Vassilliki-Alexandra Glezakou[a], Roger Rousseau[a], Yong Wang[a,b], and Robert A. Dagle[a*]

[a]*Pacific Northwest National Laboratory, P.O. Box 999, Richland, WA 99352,USA*

[b]*Voiland School of Chemical Engineering and Bioengineering, Washington State University, Pullman, WA 99164, USA*

[c]*Environmental Molecular Sciences Laboratory, Pacific Northwest National Laboratory, Richland, WA 99352,USA*

[d]*National Bioenergy Center, National Renewable Energy Laboratory, 15013 Denver West Pkwy, Golden, CO 80401,USA*

[e]*Materials Sciences Division, Lawrence Livermore National Laboratory, Livermore, CA 94550, USA*

Corresponding authors: vanessa.dagle@pnnl.gov and robert.dagle@pnnl.gov

Pyridine and Lutidine adsorption and desorption followed by Fourier Transform Infrared Spectroscopy

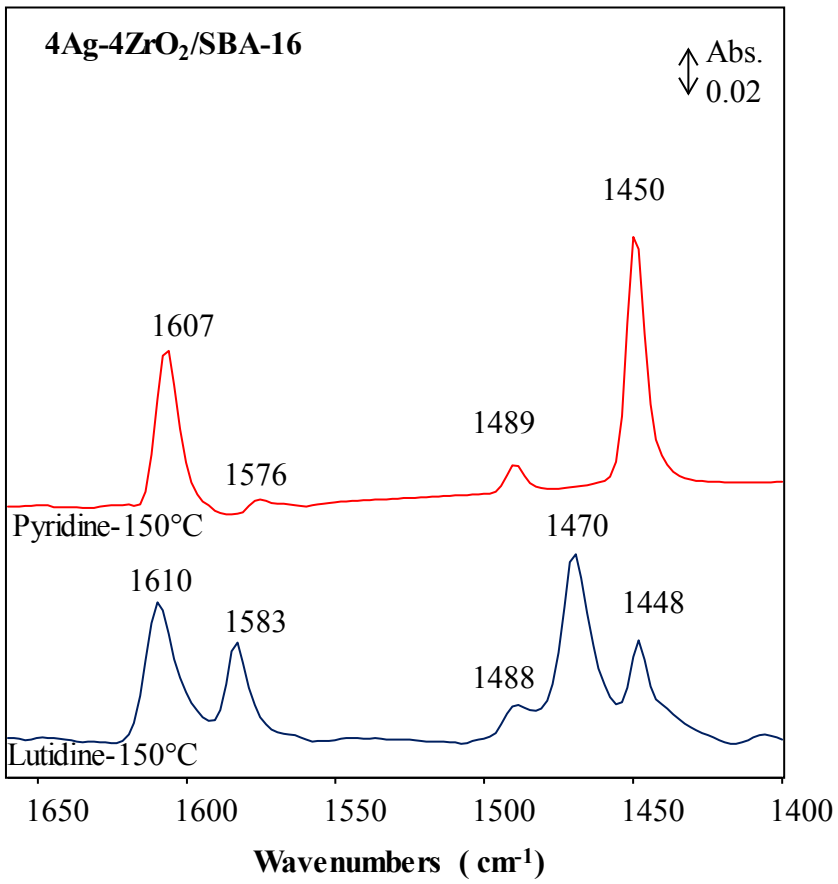

Figure S1. Infrared spectra recorded after pyridine adsorption at 50°C followed by desorption at 150°C (red spectrum) and after lutidine adsorption at 50°C followed by desorption at 150°C (blue spectrum) for 4Ag-4ZrO_2/SBA-16.

The infrared spectrum recorded after pyridine adsorption at 50°C followed by desorption at 150°C shows bands at 1607, 1576, 1489 and 1450 cm^{-1} corresponding to coordinated pyridine and characteristic of Lewis acidity.[1] No bands characteristic of Brönsted acid sites at ~ 1645 cm^{-1} and ~ 1540 cm^{-1} are detected. [2] The infrared spectrum collected after lutidine adsorption at 50°C followed by desorption at 150°C does not evidence the presence of Brönsted sites either because no doublet at ~ 1645 cm^{-1} and 1625 cm^{-1} is detected.[3, 4] Instead bands characteristics of Lutidine adsorbed on the surface by H-bonding (1610 and 1583 cm^{-1}) and bands characteristic of Lewis acid sites (1488, 1470 and 1448 cm^{-1}) are observed.[3,4]

Methods and Computational Details

Model Details

A three-dimensional periodic α-cristoballite unit cell consisting of 128 Si and 256 O atoms was used to model the SiO_2 support. A 50 atom Ag cluster corresponding to a 1 nm particle was chosen as a valid model to build the Ag-ZrO_2/SiO_2 cluster. The preoptimized Ag nanoparticle, adopted from previous studies[5-7], was preoptimized and placed on the SiO_2 support in the near proximity of a 6 atom Zr_2O_4 cluster.

The theoretical catalyst model employed in this study were designed based on previously reported TEM characterization data presented in our recent work that explores the role of Ag dispersion in selective ethanol conversion to butadiene and ethylene.[8] The TEM images showed a high degree of dispersion of Ag and ZrO_2 in the silica support with an estimated average Ag particle size of ~1.9 ± 0.8 nm. A 50 atom Ag cluster corresponding to a 1 nm particle was chosen to reflect the length scale resolution of the experimental catalyst.[8] This 50 atom Ag cluster was preoptimized and placed on the SiO_2 support in the near proximity of a 6 atom Zr_2O_4 cluster. In our previous work, we outline the use of multiple large scale AIMD simulations to perform dynamic optimization of the Ag nanoparticle on the SiO_2 support. We refer the reader to our previous study for a comprehensive discussion detailing the choice and justification of the catalyst model components, relevant preparation and structural analyses.[8] Although using the AIMD simulations does not guarantee a global minimum, dynamic optimization can lead to adopting structural configurations that have lower energy minima compared to simple static, locally optimized geometric structures.

Furthermore, the TEM images of the 4Ag/4ZrO_2/SBA16 catalyst showed amorphous, evenly dispersed ZrO_2 all over the SiO_2 support indicating that the Ag and ZrO_2 components are in near proximity with each other.[8] These ZrO_2 clusters were found to be typically ~1–3 nm and were approximately estimated to have a surface density of 0.1 Zr atoms/nm^2 catalyst based on mapping of the vdW radii of Zr and O atoms on the EDS derived images.[8]We refer the reader to our previous work for estimation of size and clustering of ZrO_2[4]. Based on the approximated experimental surface density distribution, the catalyst model limits the size of the ZrO_2 cluster to 6 atoms which corresponds to a theoretical surface coverage of 0.5 Zr atoms/nm^2. The constructed models thus mainly focus on capturing the localized effects observed in the area where both ZrO_2 and Ag moieties coexist in a 1:1 ratio, and do not represent ZrO_2 free regions of the SiO_2 support.

The resulting configuration had cell dimensions of 19.907 Å × 19.907 Å × 28.664 Å with a total of 440 atoms. A vacuum region of 20 Å was added above the SiO_2 support to avoid any spurious interaction between the top and bottom of slab model. To simulate the catalyst in the presence of

hydrogen, 8 H_2 molecules were introduced into the optimized Ag-ZrO_2/SiO_2 catalyst resulting in a simulation cell containing a total of 456 atoms with cell dimensions of 19.907 Å × 19.907 Å × 28.664 Å. Over the course of the AIMD run time, dissociative adsorption of all 8 H_2 molecules was observed accompanied with significant restructuring and redistribution of Ag atoms on the catalyst surface (Figure S1(b)).

Illustration of the Ag-ZrO_2/SiO_2 catalyst models obtained from AIMD simulations

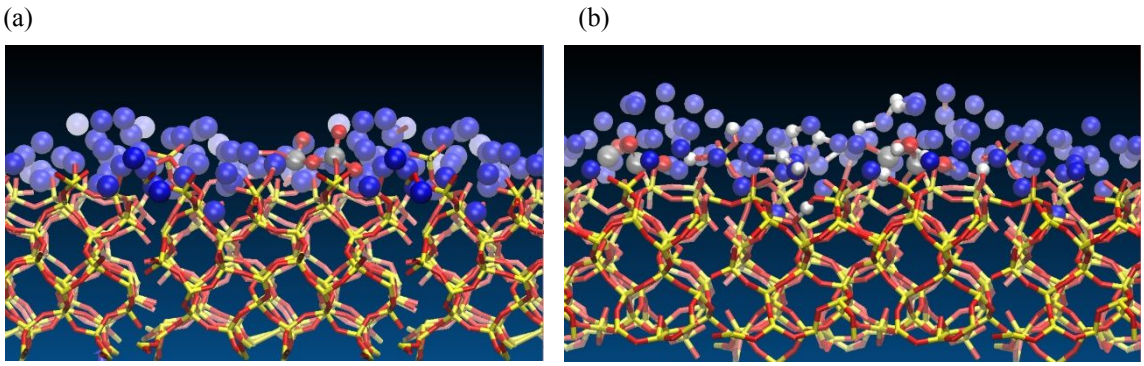

Figure S2. Simulated structures of the Ag-ZrO_2/SiO_2 catalyst models annealed using AIMD simulations in the (a) absence and (b) presence of adsorbed hydrogen. SiO_2 is depicted in cylindrical format, ZrO_2, Ag and H are displayed as spheres. Element color representations: Si (**yellow**), O (**red**), Zr (**gray**), Ag (**blue**) and hydrogen (**white**).

Atomic density distribution of species in Ag-ZrO_2/SiO_2 catalyst models

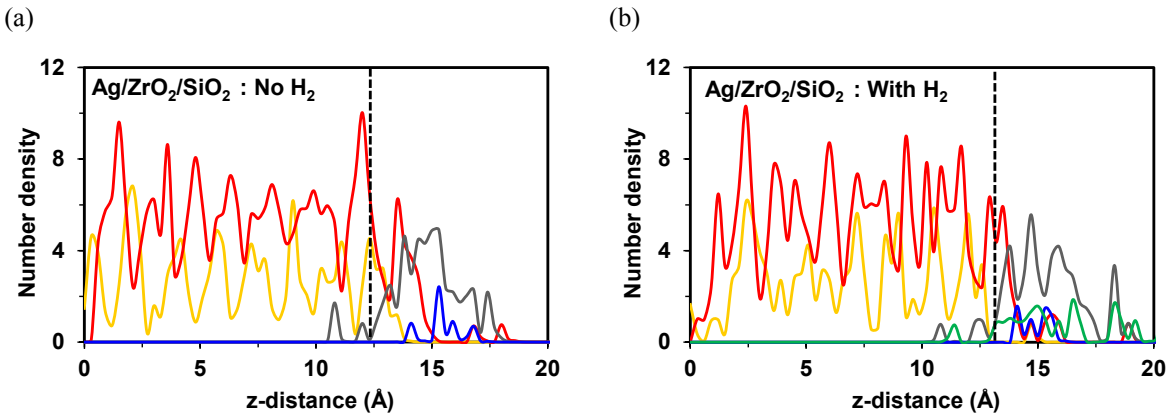

Figure S3. Atomic density profiles showing time-averaged distribution of species from AIMD simulations as a function of the surface normal direction (z) in the dispersed Ag-ZrO_2/SiO_2 catalyst models in the (a) absence and (b) presence of adsorbed hydrogen. z = 0 represents the bottom of the simulation cell. Dotted vertical line denotes the surface of the SiO_2 support. Oxygen distributions at z < dotted line denote atoms matrixed with Si (O_{SiO2}). Oxygen distributions at z > dotted line represent atoms that interface with Ag or adsorbed H atoms ($O_{Ag/H}$). Density profile color representations: Si (**yellow**), O (**red**), Zr_2O_4 (**blue**), Ag (**gray**) and H (**green**).

Effect of adsorbed hydrogen on the distribution and oxidation state of Ag in Ag-ZrO_2/SiO_2 catalyst models

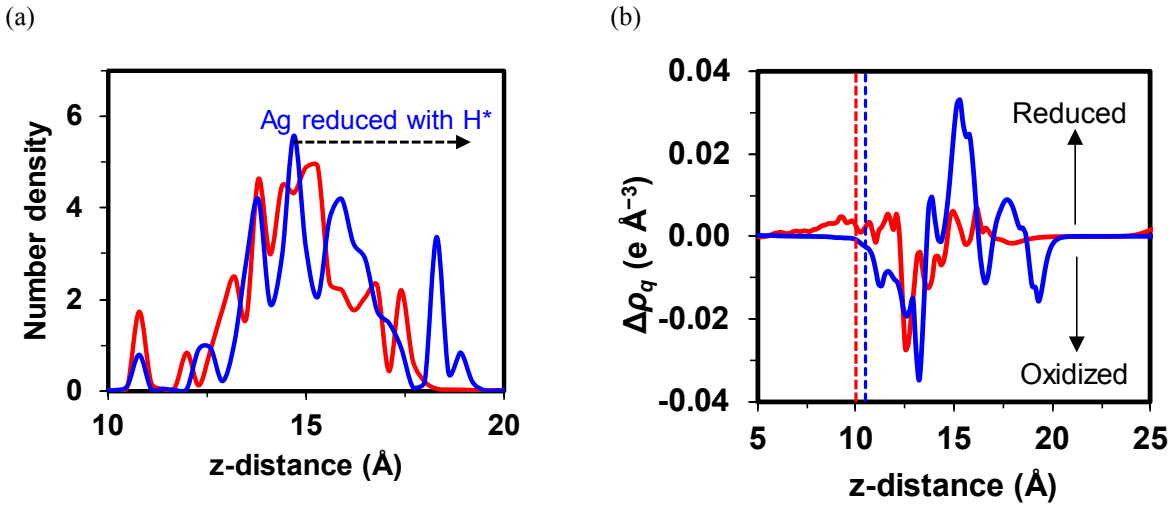

Figure S4. (a) Atomic and (b) charge density distribution (in $e^-/Å^3$) of Ag in the Ag-ZrO_2/SiO_2 catalyst models as a function of surface-normal distance (z) in the absence (**red**) and presence of adsorbed hydrogen (**blue**). Atomic densities were obtained from AIMD simulation trajectories. Positive values reflect electron gain (anionic), negative values reflect electron loss (cationic), 0 value reflects neutral (metallic). Differential electron density distribution ($\Delta\rho_q = \rho_{Total} - \rho_{Total-Ag} - \rho_{Ag}$) values were obtained from post-NVE annealed optimized strucutres. Dotted line denotes the Ag/SiO_2 interface.

Visual representation of key selectivity determining reaction intermediates on the Ag-ZrO_2/SiO_2 (H_2-free) catalyst surface in the absence of adsorbed hydrogen

(a) Crotonaldehyde + Ethanol

(b) Crotylalcohol + Acetaldehyde

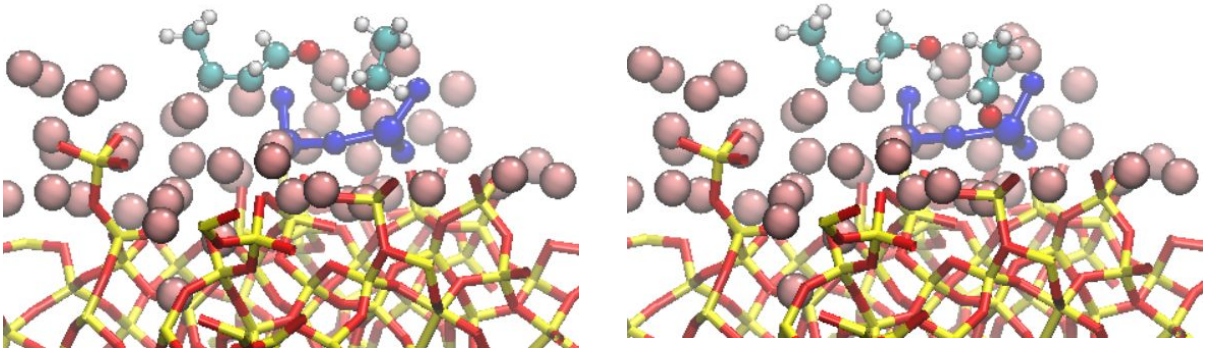

(c) Crotonaldehyde + Ethanol

(d) Butyraldehyde + Acetaldehyde

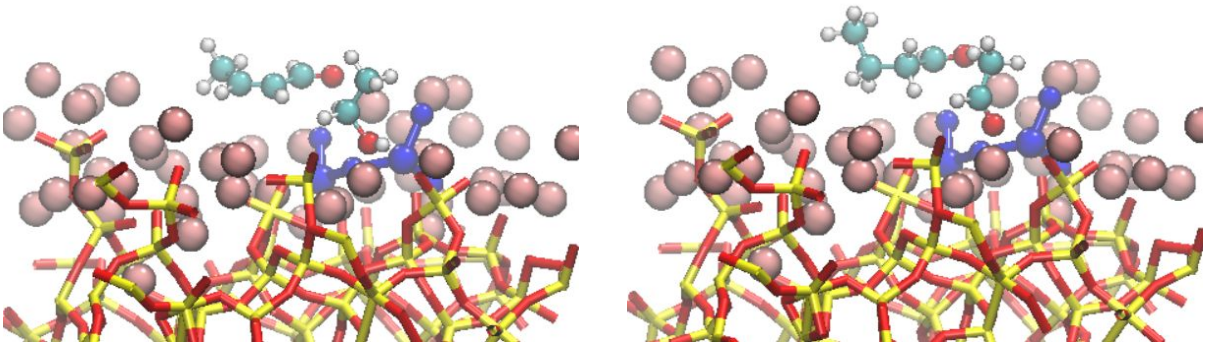

Figure S5. DFT optimized geometric configurations of reaction intermediates involved in the MPV reduction of crotonaldehyde (a) to crotyl alcohol (b) and crotonaldehyde (c) to butyraldehyde (d) on the dispersed Ag-ZrO_2/SiO_2 catalyst in the absence of adsorbed hydrogen. SiO_2 is depicted in cylindrical format, ZrO_2, Ag and hydrocarbons are displayed as spheres. Element color representations: Si (**yellow**), O (**red**), ZrO_2 (**blue**), Ag (**pink**), C (**cyan**) and hydrogen (**pearl**).

Visual representation of key selectivity determining reaction intermediates on the Ag-ZrO_2/SiO_2 catalyst surface in the presence of adsorbed hydrogen

(a) Crotonaldehyde + Ethanol

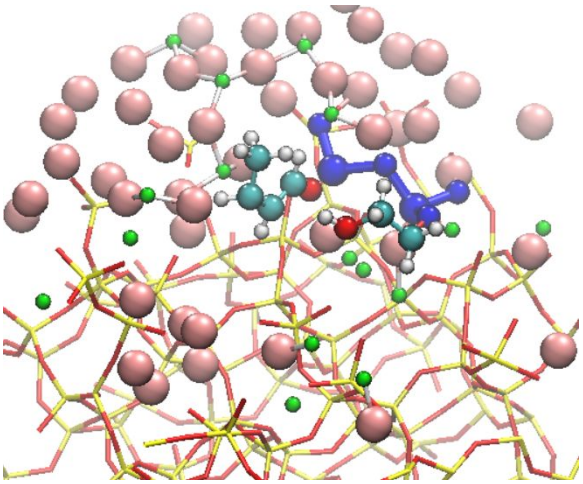

(b) Crotylalcohol + Acetaldehyde

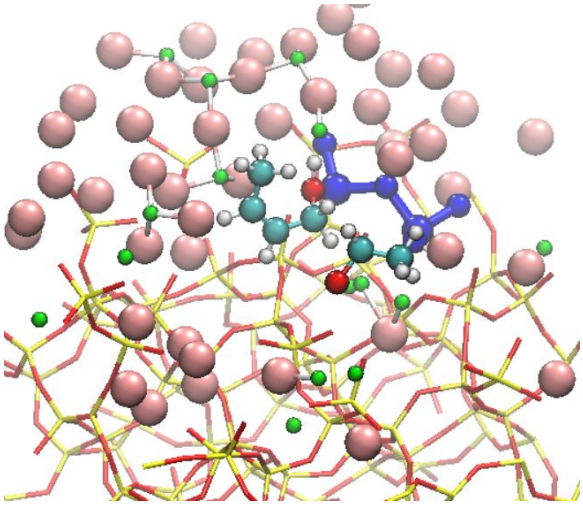

(c) Crotonaldehyde + Ethanol

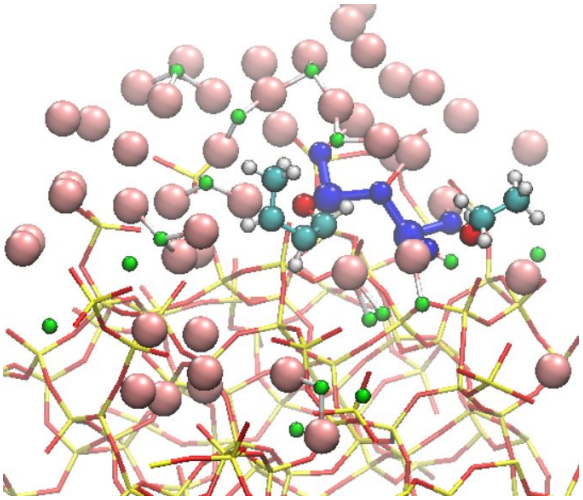

(d) Butyraldehyde + Acetaldehyde

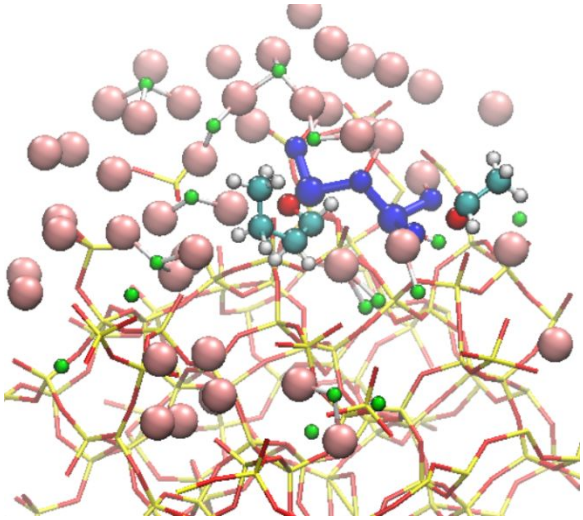

Figure S6. DFT optimized geometric configurations (top-tilted viewpoint) of reaction intermediates involved in the MPV reduction of crotonaldehyde (a) to crotyl alcohol (b) and crotonaldehyde (c) to butyraldehyde (d) on the dispersed Ag-ZrO_2/SiO_2 catalyst in the presence of adsorbed hydrogen. SiO_2 is depicted in cylindrical format, ZrO_2, Ag, hydrocarbons and surface adsorbed hydrogen are displayed as spheres. Element color representations: Si (**yellow**), O (**red**), ZrO_2 (**blue**), Ag (**pink**), C (**cyan**). Surface adsorbed hydrogen (**green**) and hydrocarbon hydrogen (**pearl**).

X-Ray Diffraction (XRD)

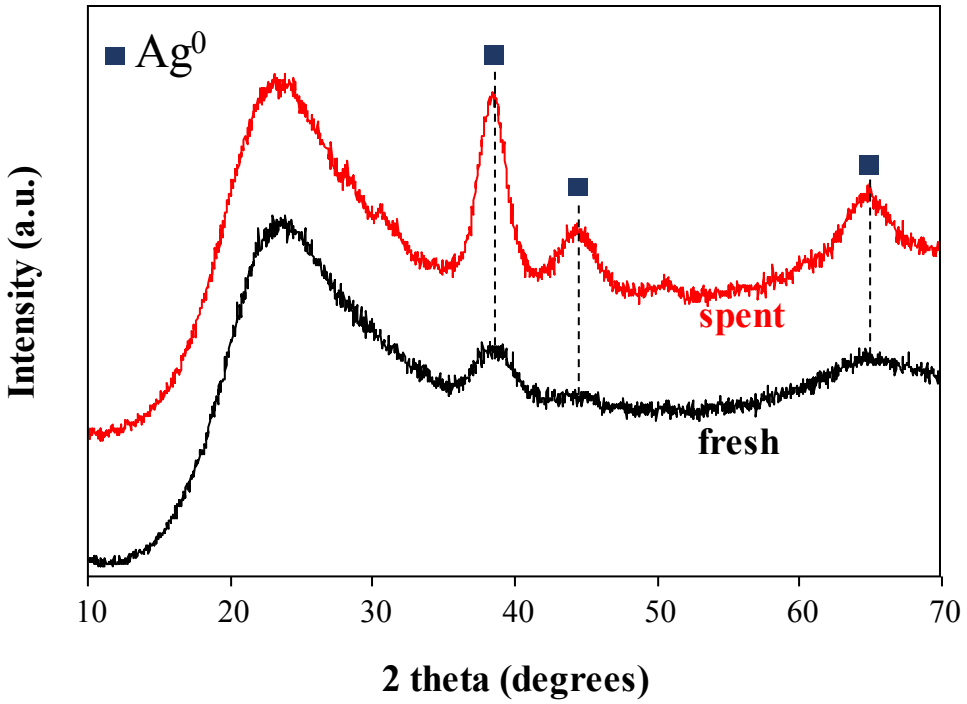

Figure S7. XRD patterns recorded for 4Ag-4ZrO_2/SBA-16. **Fresh** after reduction under 10%H_2/N_2 at 325C for 1 hour and **spent** after 180 hours on stream (Figure 6(a) of the manuscript).

X-ray powder diffraction spectra were recorded using a Philips X'pert MPD (Model PW3040/00) diffractometer with copper anode ($K\alpha_1$ = 0.15405 nm) and a scanning rate of 0.05 ° per second between 2θ = 10 °- 70 ° and 0.05 ° per 30 seconds between 2θ = 10 °- 70 °. The diffraction patterns were analyzed using Jade 5 (Materials Data Inc., Livermore, CA) and the Powder Diffraction File database (International Center for Diffraction Data, Newtown Square, PA).

The Ag° particle size was determined from the peak located at 2Θ = 38.46° using Debye-Sherrer relation ($d=0.89\lambda/ B\cos\theta$, where λ is the wavelength of Cu Kα radiation, B is the calibrated half-width of the peak in radians, and θ is the diffraction angle of a crystal face)

Transmission Electron Microscopy (TEM)

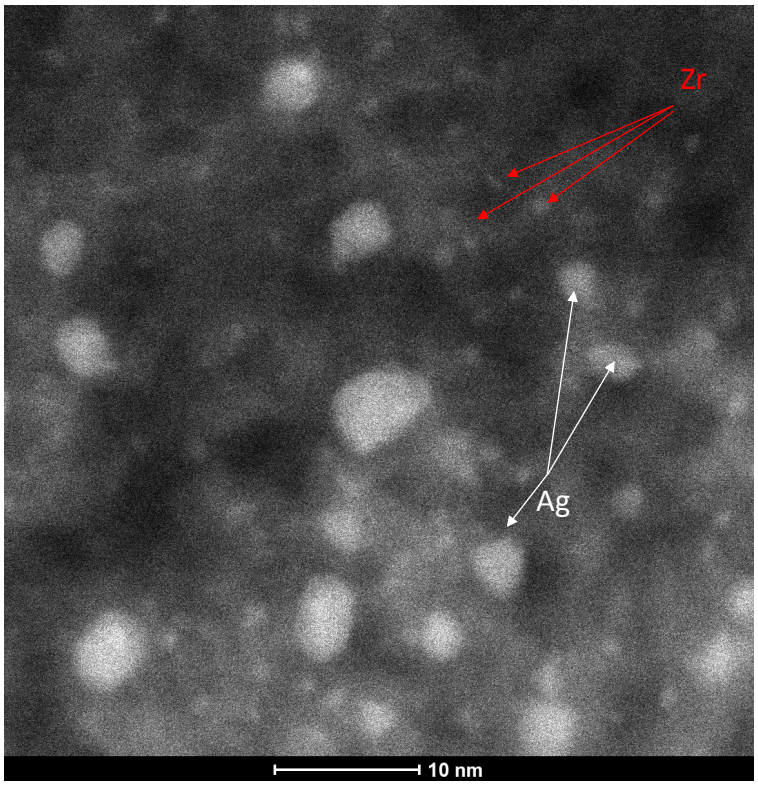

Figure S8. NAADF-STEM image for 4Ag-4ZrO_2/SBA-16 recorded after reduction at 325°C for 1 hour under 10% H_2/N_2.

Transmission electron microscopy (TEM) measurements were conducted with an FEI Titan 80-300 operated at 300 kV. All images were digitally recorded using a charge-coupled device (CCD) camera and were analyzed using Gatan Digital Micrograph. TEM images were collected from at least five different locations on the grid. In general, TEM sample preparation involved mounting powder samples on copper grids covered with lacey carbon support films and then immediately loading them into the TEM airlock to minimize an exposure to atmospheric O_2. Before measurement, samples were reduced at 325°C for 1 hour under 10% H_2/N_2.

Catalytic Performance for Butadiene hydrogenation

Table S1. Catalytic performance of 4%Ag/SBA-16 and 4%ZrO_2/SBA-16 for the hydrogenation of 1,3-butadiene.

Catalyst	Conversion (%)	Selectivities (%)- Carbon based		
		n-butene	n-butane	Others*
4%Ag/SBA-16	100	66.1	30.3	3.6
4%ZrO_2/SBA-16	75	52.7	2.2	45.1

T = 325°C, P =7 bar, H_2= 12.9 sccm, butadiene (15 wt.% in hexane) = 0.0385ml/min, catalyst = 2 grams. * mainly ethylene and Di-ethyl-ether

References

1. Onfroy, T.; Clet, G.; Bukallah, S.; Hercules, D.; Houalla, M., Development of the acidity of zirconia-supported niobia catalysts. *Catalysis Letters* **2003,** *89* (1-2), 15-19.
2. Janssens, W.; Makshina, E. V.; Vanelderen, P.; De Clippel, F.; Houthoofd, K.; Kerkhofs, S.; Martens, J. A.; Jacobs, P. A.; Sels, B. F., Cover Picture: Ternary Ag/MgO-SiO2 Catalysts for the Conversion of Ethanol into Butadiene (ChemSusChem 6/2015). *ChemSusChem* **2015,** *8* (6), 911-911.
3. Onfroy, T.; Clet, G.; Houalla, M., Quantitative IR characterization of the acidity of various oxide catalysts. *Microporous and Mesoporous Materials* **2005,** *82* (1), 99-104.
4. Elassal, Z.; Groula, L.; Nohair, K.; Sahibed-dine, A.; Brahmi, R.; Loghmarti, M.; Mzerd, A.; Bensitel, M., Synthesis and FT–IR study of the acido–basic properties of the V2O5 catalysts supported on zirconia. *Arabian Journal of Chemistry* **2011,** *4* (3), 313-319.

5. D. Mei, V.-A. Glezakou, V. Lebarbier, L. Kovarik, H. Wan, K.O. Albrecht, M. Gerber, R. Rousseau, R.A. Dagle, Highly active and stable $MgAl_2O_4$-supported Rh and Ir catalysts for methane steam reforming: A combined experimental and theoretical study, Journal of catalysis, 679 316 (2014) 11-23.

6. M. Lebarbier, D. Mei, D.H. Kim, A. Andersen, J.L. Male, J.E. Holladay, R. Rousseau, Y. Wang, Effects of La_2O_3 on the mixed higher alcohols synthesis from syngas over Co catalysts: a combined theoretical and experimental study, *The Journal of Physical Chemistry C*, 115 (2011) 17440-17451.
7. D. Mei, R. Rousseau, S.M. Kathmann, V.-A. Glezakou, M.H. Engelhard, W. Jiang, C. Wang, M.A. Gerber, J.F. White, D.J. Stevens, Ethanol synthesis from syngas over Rh-based/SiO_2 catalysts: A combined experimental and theoretical modeling study, *Journal of Catalysis*, 271 (2010) 325-342.
8. S. A. Akhade, A. Winkelman, V. L. Dagle, L. Kovarik, S. F. Yuk, M.-S. Lee, J. Zhang, A. B. Padmaperuma, R. A. Dagle, V. -A. Glezakou, Y. Wang, R. Rousseau, Influence of Ag metal dispersion on the thermal conversion of ethanol to butadiene over Ag-ZrO2/SiO2 catalysts, *Journal of Catalysis* 386 (2020): 30-38.